IEEE Access
Multidisciplinary ⋮ Rapid Review ⋮ Open Access Journal

Received 21 July 2023, accepted 2 August 2023, date of publication 7 August 2023, date of current version 14 August 2023.

Digital Object Identifier 10.1109/ACCESS.2023.3302918

RESEARCH ARTICLE

A Novel Scheme for Suppression of Human Motion Effects in Non-Contact Heart Rate Detection

ZEKUN CHEN, (Member, IEEE), YUNXUE LIU, CHENHONG SUI, (Member, IEEE), MIN ZHOU, AND YUQING SONG

School of Physics and Electronic Information, Yantai University, Yantai 264005, China

Corresponding author: Yunxue Liu (sdytrslyx@vip.163.com)

This work was supported in part by the National Natural Science Foundation of China under Grant 61601397.

ABSTRACT The technology of non-contact heart rate detection has been proven of great use. However, it is still limited by several challenges, particularly the influence of human motion and random disturbances, which significantly degrade the accuracy of the measurement. To address these challenges, this paper proposes a novel scheme for heart rate detection. Firstly, the proposed scheme utilizes the Multi-Channel Averaging (MCA) technique to improve the signal-to-noise ratio (SNR) of the extracted phase signal from the echoes in the multiple receivers, and a high-pass filter to roughly extract a heartbeat signal. Secondly, to suppress motion artifacts (MA) in the heartbeat signal caused by human motion, the Adaptive Parameter Selection for Expectation-Maximization (APSEM) method is proposed. Further, a novel processing sub-framework which combines the Kalman filtering, the Variational Mode Extraction (VME) algorithm, and the Rife spectral analysis method (called KFRV method) is proposed to mitigate the effect of random disturbances and achieve accurate frequency estimation. Experimental results using the Polar H10 heart rate sensor as a reference show that the proposed scheme achieves accurate heart rate detection in the presence of human motion, with the Mean Absolute Error (MAE) of less than 2.5 beats per minute (bpm), which is much better than traditional schemes. Compared to traditional methods, the proposed scheme exhibits negligible loss in heart rate detection under static state, with an average MAE of 0.99 bpm. Overall, the experimental results demonstrate the applicability of the proposed scheme for accurate heart rate detection in both human motion and static states.

INDEX TERMS APSEM method, frequency-modulated continuous-wave (FMCW) radar, human motion, KFRV method, MCA, non-contact heart rate detection.

I. INTRODUCTION

Heart rate (HR) is a crucial component of human vital signs which reflects an individual's physiological state. Conventional HR detection techniques rely on electrocardiogram (ECG) or photoplethysmography (PPG) [1], but these methods require physical contact with the subject, causing discomfort and potential allergy risks [2], [3], [4]. To improve the universality of long-term vital sign monitoring, research on non-contact vital sign monitoring has become a crucial area in both academia and industry [5]. Several non-contact vital sign monitoring systems have been developed using optical imaging, acoustic vibration, electromagnetic waves, and other methods [6], [7], [8]. Bio-radars have demonstrated advantages in non-contact, non-invasive, and scalable vital sign monitoring. They have been applied in various fields, including post-disaster survivor detection, sleep monitoring, and driver health evaluation in vehicles [9], [10], [11].

The radar used in non-contact vital sign monitoring is mainly composed of continuous-wave (CW) radar, impulse radio ultra-wideband (IR-UWB) radar, and frequency-modulated continuous-wave (FMCW) radar. In comparison to CW Doppler radar and IR-UWB radar, FMCW radar can divide the acquired radar signal into multiple ranges and angle

The associate editor coordinating the review of this manuscript and approving it for publication was Chengpeng Hao.

scales, and the captured information has more details [12]. Detection of vital signs using FMCW radar has become a growing area of research [13], [14], [15]. The integration of millimeter-wave (mm-wave) technology has further advanced this field. Respiration and heartbeat cause local vibrations on the body surface with amplitudes of approximately 5 mm and 200 $\mu m \sim 500\ \mu m$, respectively [16]. Due to its ability to detect small amplitude vibrations, mm-wave FMCW radar can accurately monitor vital signs.

In the current research, the advancement of various methods such as the Complete Ensemble Empirical Mode Decomposition with Adaptive Noise (CEEMDAN), the Variational Modal Decomposition (VMD), and others have led to the maturity of heart rate monitoring in the presence of the human body in a static state [17], [18], [19], [20], [21]. However, one of the significant challenges in non-contact vital sign monitoring is to achieve accurate heart rate estimation in the presence of human motion. The amplitude of human motion can interfere strongly with vital sign signals as it is much larger than the amplitude of chest displacement caused by the latter [22], [23]. Lv et al. proposed a novel scheme to enhance vital signals by utilizing the Matched filter (MF) technique to effectively eliminate interference caused by large-scale random human motion [22]. The proposed scheme operated on the fundamental principle of matched filter, which enables recovery of the input signal's information that exhibits maximum correlation with a pure template signal. By multiplying the input signal with a pure template signal devoid of human motion interference, the technique amplified the useful signal component while suppressing the noise component. Nevertheless, the effectiveness of this scheme was contingent on the purity of the selected template signal. In practical scenarios, the selected template signal may not be entirely free from the human motion, and the harmonics of the vital signal and various forms of inherent noise can further degrade the template's purity. This limitation can significantly affect the performance of the MF-based vital signal enhancement scheme. Wu et al. introduced a vital sign signal enhancement algorithm, the Multichannel-weighted Kalman Smoother (MCKS), which was designed to tackle the issue of singular values resulting from random body movements (RBM) during the vital sign monitoring [23]. The MCKS algorithm employed multiple channels of echo signals and reduced the weight of observation vectors that contain singular values through smoothing. However, the efficacy of RBM suppression using this method is influenced by the initial parameters. Inappropriate selection of initial parameters may result in incomplete RBM suppression. F. Wang and colleagues applied a MA filtering technique that employs B-spline fitting to effectively eliminate the significant interference caused by human motion [24]. The method involved employing a B-spline curve fitting strategy to model the human motion signal in the time domain, and then subtracting the fitted motion signal from the original phase signal to achieve motion artifacts removal. However, this method may be susceptible to issues of over-fitting and under-fitting, which can lead to excessive loss of valuable components in the original phase signal or incomplete removal of the human motion components. Moreover, random disturbances such as impulse noise can also degrade the accuracy of heart rate detection.

To overcome the above challenges, a novel scheme for heart rate detection using 77 GHz FMCW radar is proposed. The proposed scheme utilizes a multi-step signal processing method to obtain a stable and accurate heart rate estimation. Initially, the phase signal of the range bin where the human body is located is extracted through the signal pre-processing step. The signal-to-noise ratio (SNR) of the phase signal is then improved using Multi-Channel Averaging (MCA) and a rough heart rate signal is extracted through a high-pass filter. To address the interference caused by human motion on heart rate estimation, the Adaptive Parameter Selection for Expectation-Maximization (APSEM) method is employed to filter out the motion artifacts (MA) in the heartbeat signal. The proposed APSEM method effectively suppresses the singular values in the heartbeat signal, resulting in a reduced impact of human motion on the accuracy of heart rate detection. Further, a novel processing framework is proposed for heart rate tracking to achieve a more stable and accurate heart rate estimation. This processing framework which is called the KFRV method combines the Kalman filtering, the Rife spectral analysis method, and the Variational Mode Extraction (VME) algorithm, to suppress the effect of random disturbances on heart rate estimation and reduce heart rate deviation during heart rate detection.

The content of this paper is organized as follows: Section II introduces the preliminaries including the FMCW radar system and the fundamental theory. In Section III, the radar signal preprocessing, the APSEM method, and the KFRV method are presented. Section IV describes experiment settings parameters and results. Finally, conclusions are given in the last section.

II. PRINCIPLE OF NONCONTACT HEART RATE DETECTION BASED ON FMCW RADAR

The fundamental principle underlying the non-contact detection of vital signs using FMCW radar technology involves capturing the phase variation resulting from the motion of a target. As illustrated in Fig.1, a simplified block diagram of an FMCW radar system designed for human vital signs detection consists of several key components, including a signal generator, a power amplifier (PA), a low-noise amplifier (LNA), a low-pass filter, and an analog-to-digital converter (ADC) module.

The transmitted chirp signal can be approximately expressed as

$$x_T(t) = A_T \exp\left(j(2\pi f_{\min} t + \pi K t^2)\right), 0 < t < T_r \quad (1)$$

where $f_{\min}$ is the start frequency and K is the frequency modulation slope. A_T represents the magnitude associated with the transmit power and T_r stand for the duration of a

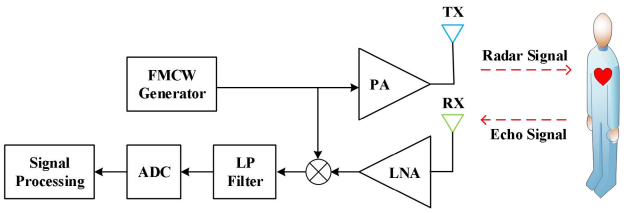

FIGURE 1. FMCW radar system block diagram.

single chirp. The signal is transmitted from the transmitting antenna (TX) to the front of the object. Afterward, the phase of $x_T(t)$ is modulated by the cardiopulmonary movement $r(t)$ due to lung and heart. The reflected signal of the receiver antenna (RX) can be expressed as

$$x_R(t) = A_R \exp\left\{j\left(2\pi f_{\min}(t-\tau) + \pi K(t-\tau)^2\right)\right\}, \quad 0 < t < T_r \tag{2}$$

$$\tau(t) = \frac{2R(t)}{c} \tag{3}$$

where $\tau(t)$ and c are the round-trip time and the velocity of the electromagnetic wave, respectively. The echo signal $x_R(t)$ can be regarded as a time delay version of $x_T(t)$, with a time delay $\tau(t)$ caused by the constant distance r_0 and the cardiopulmonary movement $r(t)$ [25]. By using the frequency mixing changed into an intermediate frequency (IF) signal, the IF signal is shown by (4).

$$\begin{aligned} S_{IF}(t) &= A_T A_R \exp\left\{j\left(2\pi K\tau t + 2\pi f_{\min}\tau - \pi K\tau^2\right)\right\} \\ &\approx A_T A_R \exp(j(2\pi f_{\min}\tau + 2\pi K\tau t)) \\ &\approx A_T A_R \exp(j(\psi(t) + 2\pi f_{IF} t)), \tau < t < T_r \end{aligned} \tag{4}$$

$$\psi(t) = 4\pi\frac{r_0 + r(t)}{\lambda}, f_{IF} = \frac{2Kr_0}{c} \tag{5}$$

In (4), the term $\pi K\tau^2$ can be neglected as the order of magnitude for this term is 10^{-6}. From (5), we can find that the change of $\psi(t)$ is apparent along with $r(t)$ relative to λ at a settled distance r_0. So, we select the phase to detect the chest wall displacement caused by heartbeat and respiration.

III. THE PROPOSED SCHEME FOR HEART RATE DETECTION

In this study, a novel scheme for heart rate detection using 77 GHz FMCW radar is proposed to tackle the issue of low accuracy in heart rate measurement caused by human motion in indoor environments. The proposed scheme utilizes a multi-step signal process to obtain a stable and accurate heart rate estimation. Initially, the phase signal of the range bin where the human body is located is extracted through the signal pre-processing step. The SNR of the phase signal is then improved using MCA, and a fourth-order Butterworth high-pass filter with a cutoff frequency of 0.8 Hz was employed to extract the heartbeat signal roughly.

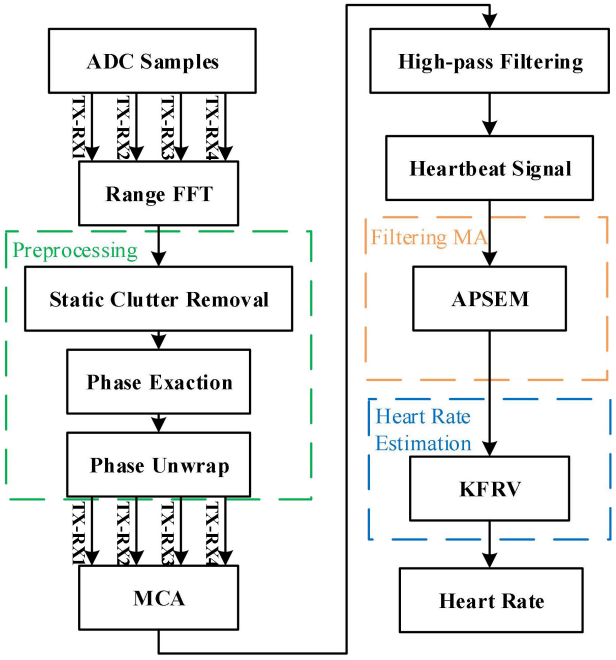

FIGURE 2. Signal processing flow.

To address the interference caused by human motion on heart rate estimation, we propose a novel method based on an adaptive initial parameters selection method and the Expectation-Maximization (EM) algorithm (called APSEM method) to filter out the MA in the heartbeat signal. The proposed ASPEM method effectively suppresses the singular values in the heartbeat signal, decreasing the effect of human motion on the accuracy of heart rate detection. Further, a novel processing sub-framework called the KFRV method is proposed for heart rate tracking to achieve a more stable and accurate heart rate estimation. This method combines the Kalman filtering, the Rife frequency measurement algorithm, and the VME algorithm, to suppress the effect of random disturbances on heart rate estimation and reduce heart rate deviation during heart rate detection. The flow chart of the proposed non-contact heart rate detection scheme is depicted in Fig.2. And the functionality of these signal processing steps is explained in the following paragraph.

A. SIGNAL PREPROCESSING

After sampling the beat signal, the Range-Fast Fourier Transform (Range-FFT) is applied to the samples of each chirp to extract the distance information of each object in the environment. The range bin corresponding to the target object is then selected. To enhance the accuracy of the range bin selection and reduce the clutter interference reflected from the static object in the measurement environment, a static clutter filtering technique is employed to eliminate the background noise. It is important to note that the phase of the echo signal reflected from static objects remains constant,

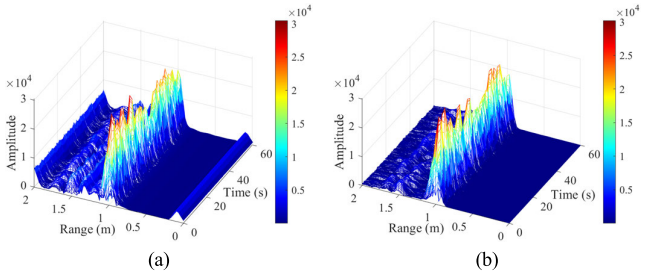

FIGURE 3. The Range-FFT results. (a) The Range-FFT results without filtering static clutter. (b) The Range-FFT results of filtering static clutter.

while human motion, such as body movements, breathing, and heartbeats, can result in changes in the distance between the radar antenna and the subject, leading to a varying phase of the echo signal [24]. Therefore, the background profile can be estimated by computing the average of the received pulses over a slow time interval and it can be denoted as

$$C(m) = \frac{1}{N}\sum_{i=1}^{N} R(m, i) \tag{6}$$

where m is the sampling point over fast-time, i is the sampling point over slow-time. Then, all the received pulses subtract the background profile, and the received pulses after filtering out static clutter can be expressed as

$$\hat{R}(m, i) = R(m, i) - C(m) \tag{7}$$

The Range-FFT of a radar signal is depicted in Fig.3, showcasing the comparison between the signal before and after static clutter removal. As evident from the figure, the removal of static clutter results in a significant reduction in background noise, thereby improving the visibility of the information related to the micro-motion target.

After filtering out static clutter, the range bin associated with the target object is selected, and the corresponding phase information is extracted for further analysis. Since this study focuses on the detection of vital signs for humans in the presence of body movements, the range bin in which the human is located changes over time. Therefore, it is necessary to update the range bin associated with the human at regular intervals to ensure accurate extraction of vital sign information. The range bin selection method employed in this study is as follows: every 128 frames, the same range bin is chosen. The selected range bin for each 128-frame segment corresponds to the range bin with the highest peak amplitude of the Range-FFT result for the first frame's data, until the next 128 frames when the range bin is updated, and so forth.

The phase value extracted directly from the data is always between $[-\pi, \pi]$, and the phase fluctuation caused by the displacement of the chest wall often exceeds this range, so the phase information obtained will have a serious wrapping phenomenon. To solve this problem, the unwrapping operation is needed to obtain the actual chest wall displacement curve. The specific process is: when the difference between the two continuous phases jumps larger than $-\pi$ or π, the latter phase adds or subtracts 2π.

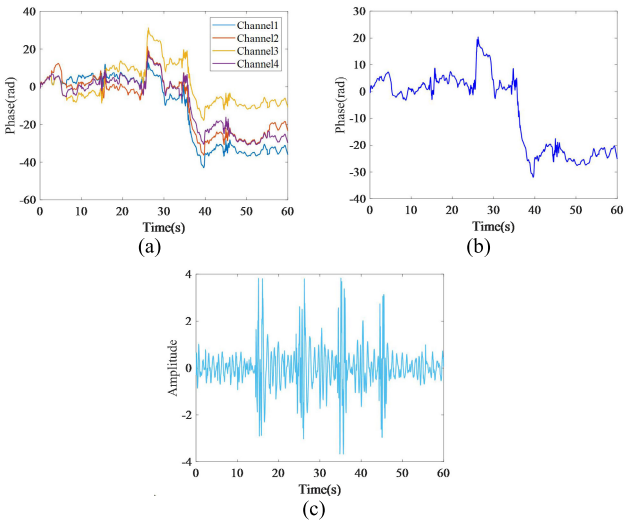

FIGURE 4. Raw data. (a) Raw data for four channels. (b) Raw data after MCA. (c) Raw data after High-Pass filter.

B. MULTI-CHANNEL AVERAGE AND ROUGH EXTRACTION OF HEARTBEAT SIGNAL

In the context of non-contact vital sign detection using radar systems, multiple receiving antennas can be employed to enhance the vital signal. The echoes obtained at each antenna contain both coherent signal components and non-coherent noise. To improve the SNR, MCA is a commonly employed technique in array signal processing [26]. In the case of 77 GHz FMCW radar systems with a multi-transmitter-multi-receiver configuration, echoes received from different transmitter-receiver pairs for a given human target contain similar heartbeat waveforms. Thus, combining the echo signals from multiple channels can improve the quality of the heartbeat signal and increase the reliability of heart rate estimation.

In this study, a system that consists of one transmitter and four receivers was utilized. After preprocessing, the phase data of the four channels were extracted. Then, after performing MCA on the phase data, a fourth-order Butterworth high-pass filter with a cutoff frequency of 0.8 Hz was employed to extract the heartbeat signal roughly. The results are depicted in Fig.4. As illustrated in Fig.4(a), the phase data of the four channels exhibit a high level of similarity. The phase data after MCA processing is presented in Fig.4(b), whereas the heartbeat signal extracted through a high-pass filter is depicted in Fig.4(c). However, as shown in Fig.4(c), despite the MCA processing, the extracted heartbeat signals still present singular values around 14 s, 25 s, 34 s, and 45 s, which are caused by human motion. It can be demonstrated that the MCA processing can't eliminate singular values in the signal, which are caused by human motion. This suggests that additional steps should be taken to either compensate for or suppress the interference caused by human motion. This highlights the limitations of MCA in these situations and the need for MA removal techniques.

C. ADAPTIVE PARAMETER SELECTION FOR EXPECTATION-MAXIMIZATION METHOD

In this paper, the APSEM method is proposed to further eliminate singular values of the heartbeat signals. The method is inspired by previous works in this field [27], [28]. In contrast to the approach taken in [27] and [28], the APSEM method provides the stopping criteria for the EM algorithm which is applied to the model established in this paper. Additionally, the APSEM method incorporates an adaptive initial parameters selection method, which is a novel enhancement to the traditional EM algorithm and serves to improve the EM algorithm's robustness.

The APSEM method considers all data samples of the heartbeat signal as observations and employs the EM algorithm to iteratively assign weights to the variance of these observations. The APSEM method utilizes iterative updates to mitigate the impact of singular values present in the heartbeat signal. Specifically, the weight assigned to the singular value component decreases with each iteration, leading to a more robust suppression of these values. This method can be applied to non-Gaussian distributed noise and suppress singular values so that a more accurate estimation of the heartbeat rate can be achieved [27]. The processing flow of the APSEM method is shown below.

First, the L data samples of the extracted heartbeat signal are modeled as a sequence of observations $[G_k]_{k=1}^{L}$, and the corresponding hidden state is denoted as $[U_k]_{k=1}^{L}$. Assuming that the system is time-invariant, the Kalman filter system equations are expressed as

$$G_k = CU_k + v_k \tag{8}$$

$$U_k = AU_{k-1} + s_k \tag{9}$$

C is the observation matrix, A is the state transfer matrix, v_k is the observation noise, and s_k is the state noise [27].

$$v_k \sim \mathcal{N}(0, R), s_k \sim \mathcal{N}(0, Q) \tag{10}$$

In this paper, v_k and s_k are assumed to be uncorrelated additive Gaussian noise with zero mean. R and Q are covariance matrices for the observation and state noise, respectively [27].

Second, a scalar weight ω_k is introduced for each observed data sample G_k such that the variance of G_k is weighted with ω_k, as done in [29]. This paper establishes the prior distribution of ω_k as a Gamma distribution to ensure that the weights remain positive [27]. Therefore, the prior relationships between the observations, state variables, and weights can be succinctly expressed as follows:

$$\omega_k \sim Gamma(a_0, b_0) \tag{11}$$

$$U_k|U_{k-1} \sim \mathcal{N}(AU_{k-1}, Q) \tag{12}$$

$$G_k|U_k, \omega_k \sim \mathcal{N}(CU_k, R/\omega_k) \tag{13}$$

In the model developed in this paper, only the observations are known, and the state variables and weights are hidden states, so the model becomes a process of solving for the hidden states. For the observations $[G_k]_{k=1}^{L}$, the posterior distribution of state variables and weights can be estimated by maximizing the log-likelihood $\log(U_{1:L}, G_{1:L}, \omega_{1:L})$, and the model can be solved by the EM algorithm [28].

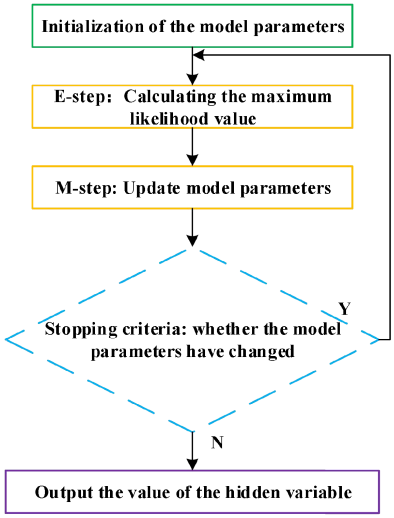

FIGURE 5. The EM algorithm flow chart.

The EM algorithm is a widely-utilized method for estimating hidden variables in probabilistic models. The fundamental flow of this algorithm is depicted in Fig.5 and can be outlined as follows:

1) Initialization: The hidden variables to be estimated are initialized, and their initial distribution is utilized.
2) E-Step: The initial distribution of the hidden variables is used to calculate the Maximum Likelihood Estimates (MLEs) of these variables, yielding the posterior estimates of the hidden variables.
3) M-Step: The MLEs obtained in the E-Step are then maximized to update the parameters of the hidden variable distribution.
4) Iteration: This process of E-Step and M-Step is repeated until the parameters of the model no longer change. The stopping condition is usually determined by monitoring the convergence of the model's parameters.

The hidden variables in the model developed in this paper are $[U_k]_{k=1}^{L}$ and $[\omega_k]_{k=1}^{L}$, and their true posterior distributions should be used to calculate the maximum likelihood estimation in the sequence. The expectation of the complete data likelihood should be taken concerning the true posterior distribution of all hidden variables [27]. However, since this is an analytically intractable expression [23], we make a factorial approximation of the true posterior as follows:

$$p([U_k]_{k=1}^{L}, [\omega_k]_{k=1}^{L}) = \prod_{k=1}^{L} p(\omega_k)p(U_{k+1}|U_k)p(U_1) \tag{14}$$

The EM algorithm, based on Gaussian and gamma distributions, proceeds with the following steps once the model parameters have been initialized:

E-step: Calculating the maximum likelihood value and solving the posterior estimates of the hidden variables. When $k = 2$, the E-step solution starts and iterates until $k = L$.

$$E_k = (\omega_k C^T R^{-1} C + Q^{-1})^{-1} \tag{15}$$

$$U_k = E_k(Q^{-1} A U_{k-1} + \omega_k C^T R^{-1} G_k) \tag{16}$$

$$\omega_k = \frac{a_{\omega_k,0} + 0.5}{b_{\omega_k,0} + \left((G_k - CU_k)^T R^{-1} (G_k - CU_k)\right)} \tag{17}$$

In the E-step, (15) denotes the posterior variance of the state variables, (16) denotes the posterior mean of the state variables, and (17) represents the update expression for the weights.

M-step: Update model parameters.

$$C = (\sum_{k=2}^{L} \omega_k G_k U_k^T)(\sum_{k=1}^{L} U_{k-1} U_{k-1}^T)^{-1} \tag{18}$$

$$A = (\sum_{k=1}^{L} U_k U_{k-1}^T)(\sum_{k=1}^{L} U_{k=1} U_{k=1}^T)^{-1} \tag{19}$$

$$R = \frac{1}{L} \sum_{k=1}^{L} \omega_k (G_k - CU_k)^2 \tag{20}$$

$$Q = \frac{1}{L} \sum_{k=1}^{L} (U_k - AU_{k-1})^2 \tag{21}$$

In the EM algorithm, the updated parameters obtained in the M-step are utilized in the computation of the E-step in the subsequent iteration. The updated expression for weight ω_k incorporates the deviation between the predicted and observed values, represented as $G_k - CU_k$ in the denominator. If this deviation is substantial, the weight ω_k will decrease in magnitude. In the case where the deviation becomes infinite, ω_k approaches zero, implying that the observations at this point have no effect on the optimal estimation of the model parameters. Hence, the EM algorithm employed in this paper can effectively suppress the interference of singular values that arise from human motion.

Unlike the literature [27], [28], the stopping criteria for the EM algorithm, applied to the established model in this study, are presented to guarantee convergence. The stopping criteria are expressed as follows:

$$\left|R_{cur} - R_{pre}\right| < \lambda R_{pre} \& \left|Q_{cur} - Q_{pre}\right| < \lambda Q_{pre} \tag{22}$$

where R_{cur}, Q_{cur} denote the observation noise and state noise of the current M-step update, respectively, and λ is the threshold value of the stop condition. Additionally, R_{pre}, Q_{pre} denote the observation noise and state noise of the last M-step update, respectively. In this paper, we set the maximum number of iterations for the EM algorithm to 1000 and the stopping criteria threshold value λ for the iterations to 0.01. When the stopping criteria are satisfied, the EM algorithm iteration stops, and the heartbeat signal sequence $[Z_k]_{k=1}^{L}$ can be obtained after removing the singular values. The above-described method for filtering motion artifacts can be referred to as the EM method.

$$[Z_k]_{k=1}^{L} = C\,[U_k]_{k=1}^{L} \tag{23}$$

Fig.6 presents the comparison of heartbeat signals before and after motion artifact filtering, along with their respective

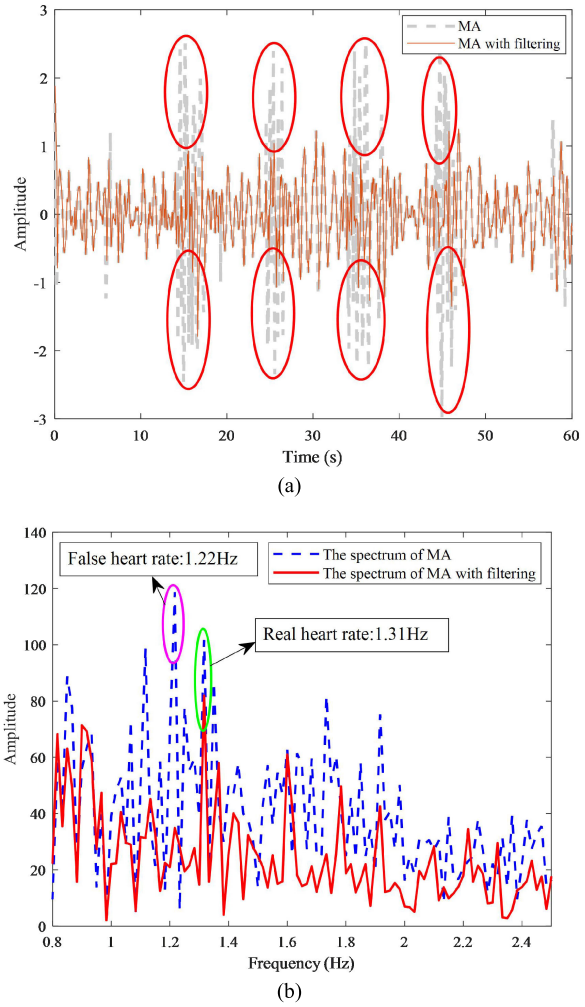

FIGURE 6. The heartbeat signal and its spectrum. (a) The heartbeat signal before and after filtering out MA. (b) The spectrum of the heartbeat signal before and after filtering out MA.

spectral analysis. As depicted in Fig.6(a), the gray dashed line represents the raw heartbeat signal, which contains a significant number of singular values due to human motion. These singular values are marked with red circles in the figure. The solid orange line shows the heartbeat signal filtered by the EM method, which indicates the absence of singular values after processing and the effective suppression of human motion artifacts in the heartbeat signal.

The blue curve in Fig.6(b) represents the spectrum of the heartbeat signal without motion artifacts filtering, while the red curve represents the spectrum of the heartbeat signal processed by the EM method. The average heart rate of the subject, as measured by the Polar H10 chest heart rate sensor, was found to be 78.4 beats per minute (bpm), or approximately 1.31 Hz. The actual heartbeat spectrum peak, indicated in the figure by a green circle, corresponds to a frequency of 1.32 Hz in the spectrum. The blue curve reveals that the real heartbeat spectrum peak is obscured by the peak corresponding to 1.22 Hz, leading to an error of 5.2 bpm in heart rate

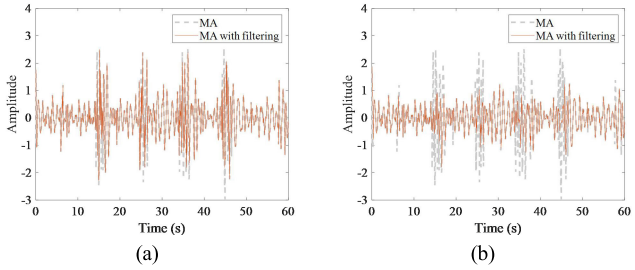

FIGURE 7. Comparison of the effectiveness of EM methods for filtering MA with different initial parameters. (a) The initial parameters are $\langle a_0 = 0.5, b_0 = 0.5\rangle$. (b) The initial parameters are $\langle a_0 = 0.25, b_0 = 0.5\rangle$.

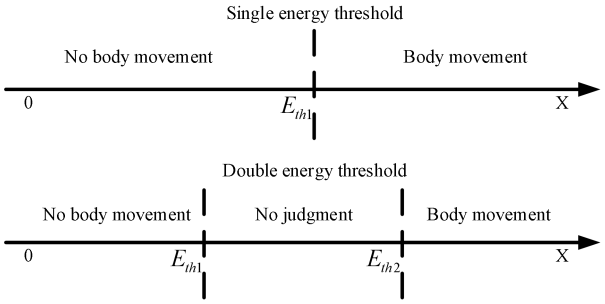

FIGURE 8. Two energy threshold methods to judge human motion.

measurement using the spectral analysis method. However, as can be seen from the red curve, motion artifacts filtering effectively suppresses the peak associated with 1.22 Hz, thus allowing the real heartbeat spectrum peak to take center stage. The heart rate result obtained through spectral analysis after motion artifacts filtering is only 0.8 bpm error compared to the typical heart rate measurement provided by the heart rate sensor.

The EM method for filtering out motion artifacts has been shown to be effective through experimentation and analysis. Before performing the EM method, we need to select appropriate initial Gamma distribution parameters. In the following, we discuss the impact of initial Gamma distribution parameters for MA suppression.

The effect of the motion artifacts suppression for a set of heartbeat signals with human motion is presented in Fig.7 for two different initial Gamma distribution parameters sets. The initial parameters are $\langle a_0 = 0.5, b_0 = 0.5\rangle$ in Fig.7(a) and $\langle a_0 = 0.25, b_0 = 0.5\rangle$ in Fig.7(b). A comparison of these two figures reveals that, when the initial Gamma distribution parameters are set to $a_0 = 0.5, b_0 = 0.5$, many singular values remain after motion artifact filtering and the interference generated by human motion is not effectively suppressed. However, when the initial Gamma distribution parameters are set as $a_0 = 0.25, b_0 = 0.5$, there is a significant reduction in the singular values caused by human motion in the heartbeat signal, resulting in a notable improvement in the motion artifact filtering effect. These experimental results and analysis demonstrate that the selection of the initial Gamma distribution parameter significantly affects the EM method's ability to suppress MA.

This is because the effect of human motion and electromagnetic environments are very sophisticated, so it is unlikely that a single set of initial parameters will be suitable for processing all signals. In cases where a set of heartbeat signals are significantly disturbed by human motion and contain multiple singular values, it is possible that the EM method can't delete any effect of human motion by setting the wrong initial prior distribution parameters ($a_{\omega_k,0}$ and $b_{\omega_k,0}$).

Consequently, this paper proposes a novel method for adaptive selection of the initial Gamma distribution parameter for the EM method. The proposed method adopts a double energy threshold detector to determine the strength of the human motion, which can indirectly provide information about the strength of the singular values in the heartbeat signal. Subsequently, adaptively adjust the initial parameters of the Gamma distribution based on the a priori information of the strength of these singular values. According to (17), when the degree of human motion is strong, the ratio of the initial parameters a_0 and b_0 in the Gamma distribution should be reduced appropriately to suppress the stronger singular values better. Conversely, when human motion is weak, the opposite is true.

The double energy threshold detection method is based on traditional energy detection with only one threshold, which can further increase the detection performance [30]. The difference between the double energy threshold detection method and the traditional single energy threshold detection method is shown in Fig.8.

The procedure for detecting human motion with double energy thresholds is as follows. Assuming that $x(i)$ denotes the magnitude of the ith sampling point of the heartbeat signal, the energy statistic detected at this point is obtained by calculating the energy sum of the M sample points in the vicinity of this sample point as

$$E_i = \sum_{i=1}^{M} |x(i)|^2 \tag{24}$$

The obtained energy statistics are compared with the two energy thresholds E_{th1}, E_{th2}, and a decision is made on whether a body movement has occurred. During the actual signal acquisition, if the calculated energy value is larger than E_{th1} and less than E_{th2}, this signal segment will not be judged as occurring human motion. The judgment result D_i can be expressed as follows

$$D_i = \begin{cases} -1, E_i < E_{th1} \\ 0, E_{th1} < E_i < E_{th2} \\ 1, E_i > E_{th2} \end{cases} \tag{25}$$

where D_i equals 1, it signifies that no human motion occurs, whereas if D_i equals 0, no judgment is made, and a value of -1 indicates the presence of human motion [30].

The threshold values E_{th1} and E_{th2} of the double threshold energy detection are determined by the statistical mean and

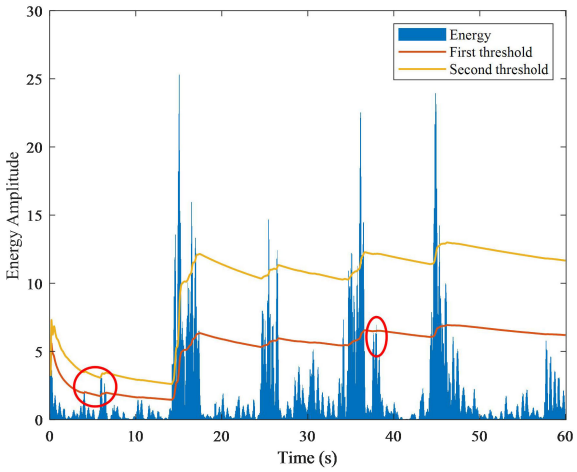

FIGURE 9. Short-time energy change of the heartbeat signal.

standard deviation of the signal energy in the absence of human motion in the previous period.

$$\begin{cases} E_{th1}(k) = E_{mean}(k-1) + \beta_1 E_{std}(k-1) \\ E_{th2}(k) = E_{mean}(k-1) + \beta_2 E_{std}(k-1) \end{cases} \tag{26}$$

where $E_{th1}(k)$ and $E_{th2}(k)$ denote the two threshold values at the kth sampling point of the heartbeat signal, $E_{mean}(k-1)$ denotes the mean value for the previous $k-1$ energy values, and $E_{std}(k-1)$ denotes the standard deviation for the previous $k-1$ energy values. Additionally, β_1 and β_2 are two weighting factors, which empirically take the values of 1.1 and 2.6, respectively.

Experiments were performed to evaluate the efficacy of the double energy threshold method for detecting human motion during heart rate monitoring. Some 60-second monitoring experiments were conducted on volunteers, who were instructed to perform four distinct movements (forward, backward, shoulder shaking, and arm swinging) at 15 s, 25 s, 35 s, and 45 s, respectively, and each movement lasted approximately 2 s, after which the volunteers returned to a static reference position. Fig.9 demonstrates the accuracy and effectiveness of the double energy threshold method in detecting these body movements during noncontact heart rate monitoring. As illustrated in the figure, it is noticeable that some energy values exceed the first threshold even when the human is in a static state, as indicated by the red circles. This highlights the potential for erroneous decisions when relying on a single threshold. In contrast, the results shown in Fig.9 demonstrate that the double energy threshold method accurately detects body movements with moments and durations consistent with the experimental setting. Extensive experiments reveal that the double energy threshold detection method is accurate and effective for detecting human motion during noncontact heart rate monitoring.

After double threshold energy detection, the percentage of body motion duration to the total duration of the heartbeat signal t_{out} is calculated; subsequently, the ratio E_r of the maximum energy at the heartbeat signal to its corresponding energy threshold E_{th2} is found. The motion model is classified into five modes considering the above two indicators of t_{out} and E_r in this paper. The motion model and the related evaluation criteria are shown in Table 1.

TABLE 1. Human motion models discrimination.

Motion model	Evaluation Indicator
Model 1 High-level body motion	$t_{out} > 8\% \,\&\, E_r \geq 2$
Model 2 Medium-level body motion	$t_{out} > 8\% \,\&\, E_r < 2$
Model 3 Low-level body motion	$4\% < t_{out} \leq 8\%$
Model 4 Weak-level body motion	$t_{out} \leq 4\% \,\&\, E_r \geq 2.5$
Model 5 Almost no body motion	$t_{out} \leq 4\% \,\&\, E_r < 2.5$

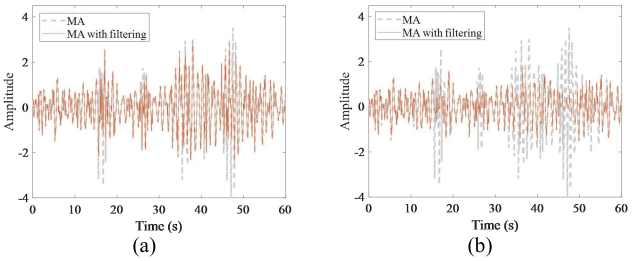

FIGURE 10. Comparison of the effectiveness of the EM method with default initial parameters and the APSEM method for filtering MA. (a) The EM method with default initial parameters for filtering MA. (b) the APSEM method for filtering MA.

After determining the motion mode of the current heartbeat signal, it is necessary to identify the corresponding initial Gamma distribution parameters of the EM method. Extensive experiments have been done to investigate the appropriate value of initial Gamma distribution parameters corresponding to the different motion modes, the typical value can be given as

$$Gamma = \begin{cases} \langle a_0 = 0.15, b_0 = 0.5 \rangle, Model1 \\ \langle a_0 = 0.2, b_0 = 0.5 \rangle, Model2 \\ \langle a_0 = 0.25, b_0 = 0.5 \rangle, Model3 \\ \langle a_0 = 0.3, b_0 = 0.5 \rangle, Model4 \\ \langle a_0 = 0.5, b_0 = 0.5 \rangle, Model5 \end{cases} \tag{27}$$

After double threshold energy detection, t_{out}, E_r can be calculated, and the human motion model can be identified based on Table 1. Consequently, the initial Gamma distribution parameters can be selected adaptively based on the human motion model.

Fig.10 illustrates a comparison between the motion artifacts removal effects achieved using the EM method with default initial distribution parameter of $\langle a_0 = 0.3, b_0 = 0.5 \rangle$ and the APSEM method for the same set of heartbeat signals.

The solid orange line represents the signal with motion artifacts filtered out, while the dashed grey line represents the signal without filtered motion artifacts. Fig.10(a) illustrates that when the default initial distribution parameter is

employed, the signal processed by the EM method is nearly identical to the original signal, with a significant number of singular values still present. On the other hand, Fig.10(b) shows that when the adaptive parameter selection method is employed to select the initial distribution parameter, the EM method is more effective in removing motion artifacts, suppressing most of the singular values due to human motion. The specific processing is that the heartbeat signal depicted in Fig.10 was classified as Model 1 (High-level body motion) by the motion model classification method based on the double energy threshold. Subsequently, the corresponding initial Gamma distribution parameter was selected as $\langle a_0 = 0.15, b_0 = 0.5\rangle$.

The motion artifacts filtering method, which combines adaptive parameter selection with the EM method, is referred to as the APSEM method in this paper. In the context of heart rate monitoring with human motion, the APSEM method offers improvements over the EM method, as it eliminates the requirement for adjusting parameters and enhances the robustness of the traditional EM method.

D. VARIATIONAL MODE EXTRACTION ALGORITHM

In 2014, Dragomiretskiy and Zosso presented a novel VMD algorithm for signal processing [19]. The VMD algorithm enables the specification of the number of modes required for signal decomposition and facilitates the separation of signal components with well-defined characteristics. Additionally, the VMD algorithm addresses the issue of modal mixing and provides modal components with independent center frequencies and sparse representations in the frequency domain. The VMD algorithm has gained widespread usage for extracting vital sign signals and has been shown to significantly improve the SNR of these signals.

However, the VMD algorithm has some limitations, including computational intensity, making real-time analysis of signals challenging, and the difficulty in selecting an appropriate number of modes. If the number of modes in the data is unknown, it can be challenging to select the right number of modes, which can result in either modal confusion or the appearance of invalid and false components in the decomposition results. These limitations hinder the application of the VMD algorithm for the analysis of vital signs signals.

The VME algorithm, proposed by Nazari and Sakhaei in 2018, is an improved approach for extracting specific mode signals from ECG signals [31]. The algorithm is designed to overcome the limitations of the traditional VMD algorithm, with advantages such as low time complexity and the absence of a requirement to determine the number of modes beforehand. Due to the priori frequency distribution range of heartbeat signals and the VME algorithm's capacity for extracting the specific mode, the VME algorithm enables accurate extraction of the heartbeat signal with a very low computational burden. Consequently, we adopt the VME algorithm to extract the accurate heartbeat signal after removing motion artifacts. The theoretical derivation of the VME algorithm is described in [31], and the specific implementation process of the algorithm is summarized as follows.

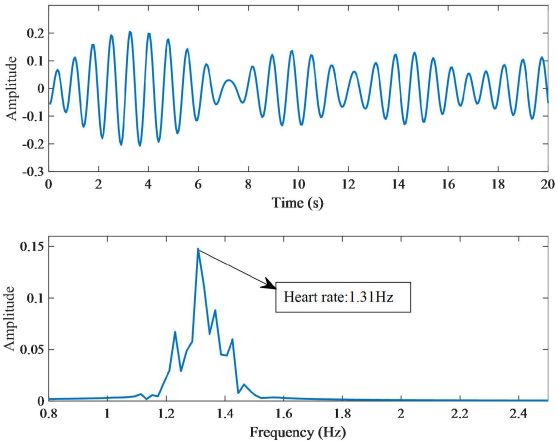

FIGURE 11. The heartbeat signal is extracted by the VME algorithm and its spectrum.

Algorithm 1 VME

Input: Initialize $u_d^1, \lambda^1, \omega_d, n \leftarrow 0$, ω_d represents the center frequency of the desired mode.

Repeat: $n \leftarrow n + 1$

1) Update u_d for all $\omega \geq 0$:
$$u_d^{n+1}(\omega) = \frac{f(\omega)+\alpha^2(\omega-\omega_d^{n+1})^4 u_d^n(\omega)+\lambda(\omega)/2}{\left[1+\alpha^2(\omega-\omega_d^{n+1})^4\right]\left[1+2\alpha(\omega-\omega_n^d)^2\right]}$$
2) Update ω_d:
$$\omega_d^{n+1} = \frac{\int_0^\infty \omega\left|u_d^{n+1}(\omega)\right|^2 d\omega}{\int_0^\infty \left|u_d^{n+1}(\omega)\right|^2 d\omega}$$
3) Dual Ascent for all $\omega \geq 0$:
$$\lambda^{n+1} = \lambda^n + \tau\left[\frac{f(\omega)-u_d^{n+1}(\omega)}{1+\alpha^2(\omega-\omega_d^{n+1})^4}\right]$$

Until: $\frac{\left\|u_d^{n+1}-u_d^n\right\|_2^2}{\|u_d^n\|_2^2} < \varepsilon$

Output: u_d^{n+1}

The output heartbeat signal of the VME algorithm and its spectrum are presented in Fig.11.

E. HEART RATE ESTIMATION METHOD

For the heartbeat signal obtained by the VME algorithm, a spectrum estimation method is necessary for estimating the frequency of the heartbeat signal. The FFT algorithm is widely used for heart rate estimation, but its estimation accuracy is limited. The Rife algorithm is a classical frequency measurement method widely used for the accurate estimation of instantaneous frequency in electromagnetic countermeasure (ECM). Reference [32], the Rife algorithm employs the maximum and the sub-maximum values in the whole amplitude spectrum of a signal to interpolate the accurate frequency. In this paper, we first exploit the Rife algorithm to

attain a more accurate estimation of heartbeat rate, and Rife is performed after FFT processing. In addition, after the FFT of the heartbeat signal, only the maximum spectral line value is found within the corresponding frequency range [0.8, 2.5] Hz of a normal human heartbeat for interpolation.

Heart rate is varying from 48 to 150 bpm, so the frequency of the heartbeat signal is in the range of [0.8, 2.5] Hz. After FFT processing of the heartbeat signal, only the maximum peak of its amplitude spectrum spectral line value within the range of [0.8, 2.5] Hz is selected to perform the Rife algorithm for calculating heart rate. Assuming that the sampling frequency of the heartbeat signal is f_s, the N-point FFT is performed for heartbeat signals, and the corresponding frequency range of the heartbeat signal is $[f_1, f_2]$, where $f_1 = 0.8$ Hz, $f_2 = 2.5$ Hz. The maximum peak of the amplitude spectrum spectral line value $|X(k_0)|$ lies in the range $\left[\frac{Nf_1}{f_s}, \frac{Nf_2}{f_s}\right]$ is selected to perform the Rife algorithm, and the sub-maximum spectrum line value $|X(k_0 + r)|$ around the maximum spectrum line value $|X(k_0)|$ is used for interpolation. The estimated heartbeat signal frequency f_h is expressed as

$$f_h = \frac{f_s}{N}\left[k_0 + r \cdot \frac{|X(k_0 + r)|}{|X(k_0)| + |X(k_0 + r)|}\right] \tag{28}$$

when $|X(k_0 + 1) \gtrless |X(k_0 - 1)|$, $r = \pm 1$.

The APSEM method proposed in the previous section enables the removal of the interference caused by human motion, the primary challenge now becomes achieving accurate heart rate estimation in the presence of the human body in a static state. In heart rate measurement and tracking, relying solely on the Rife spectral analysis method does not eliminate the influence of random disturbances such as impulse noise and RBM. To enhance the accuracy and stability of heart rate detection, this paper proposes a novel sub-framework combining the Kalman filter with the Rife spectral analysis method and the VME algorithm which is called the KFRV method. This sub-framework is supported by existing literature [33], [34]. The use of the Kalman filter is expected to effectively mitigate the impact of unknown disturbances, leading to improved performance in heart rate tracking. In conclusion, the KFRV method aims to address inaccuracies in heart rate detection caused by random interference in the presence of the human body in a static state. Furthermore, we have combined the APSEM method and the KFRV method to establish a novel scheme for non-contact heart rate detection.

The KFRV involves several signal processing steps. First, the extracted heartbeat signal by the VME algorithm is processed by sliding window, and the Rife algorithm is applied to determine the heart rate in this time window as the observed value. Subsequently, Kalman filtering is performed on the observed value within the current sliding window and the predicted value obtained from the previous window to arrive at an accurate heart rate estimate. This methodology assumes that both the observed noise and the system noise follow Gaussian distributions, as is assumed in Kalman filtering. The concrete functions of these signal processing steps for the KFRV are explained in the following paragraph.

The state vector in KFRV is expressed as

$$O = \begin{bmatrix} h & h' & h'' \end{bmatrix}^T \tag{29}$$

where variables h, h', h'' correspond to the heart rate in Hertz, its first-order derivative, and second-order derivative, respectively [34]. The state vector in a Kalman filter, represents at a sliding window k, is characterized by a Gaussian process with a mean, denoted by $O_{k|k}$, and a covariance matrix, denoted by $P_{k|k}$.

In the KFRV, we have designed a Kalman filtering process using a constant acceleration model, with the corresponding state transition matrix denoted as S. Using this state transition matrix S, we can predict the state vector for the $k+1$th sliding window based on the state vector of the kth sliding window as follows:

$$O_{k+1|k} = SO_{k|k} = \begin{bmatrix} 1 & \Delta T & \Delta T^2 \\ 0 & 1 & \Delta T \\ 0 & 0 & 1 \end{bmatrix} O_{k|k} \tag{30}$$

where ΔT represents the time interval between two consecutive sliding windows. The observation model is provided as

$$Y_{k+1} = IO_{k+1|k} = \begin{bmatrix} 1 & 0 & 0 \end{bmatrix} O_{k+1|k} \tag{31}$$

in which I denotes the observation matrix.

The measured heart rate estimation value obtained from the Rife algorithm is represented as z_{k+1}. Specifically, z_{k+1} represents the frequency of the heartbeat signal measured by the Rife algorithm within the $k+1$th sliding window, which is utilized as an observation in the Kalman filtering process. In the Kalman filtering procedure, the Q and R noise matrices are specified in [34]. In this paper, the two-point differencing method is employed to select the initial values for the Kalman filtering process [35]. Upon the initial recording of vital data, a tracking process is initiated using default Q and R noise matrices, as well as the initial state $O_{0|0}$ and covariance $P_{0|0}$. The KFRV then operates at each successive sliding window k as described below.

1) Heartbeat signal extraction: The accurate heartbeat signal is extracted by the VME algorithm from the signal after removing motion artifacts.
2) Rife frequency measurement: The heart rate estimation z_{k+1} is obtained in the frequency domain through the Rife spectral analysis method.
3) State prediction:

$$O_{k+1|k} = SO_{k|k} \tag{32}$$

$$P_{k+1|k} = SP_{k|k}S^T + Q \tag{33}$$

4) Ellipsoidal gating:

$$Y_{k+1} = IO_{k+1|k} \tag{34}$$

$$(z_{k+1} - Y_{k+1})^T P_{k+1|k}^{-1}(z_{k+1} - Y_{k+1}) \gtrless \gamma \tag{35}$$

TABLE 2. Radar parameters.

Parameter	Value
Start Frequency	77 GHZ
Idle Time	7 μs
ADC Sampling time	50 μs
Band Width	3.99 GHZ
Frame Frequency	20 HZ
Chirp Numbers	2
ADC Samples	200

where γ is the ellipsoidal gate constant. The ellipsoidal gating function assesses whether the heart rate estimate z_{k+1} falls within the established gating window. If the estimate falls outside of this ellipsoidal window, the Kalman filter is not updated as the estimate is considered an outlier. Conversely, if the estimate falls within the gating window, the Kalman filter is updated [34].

5) Kalman filter state update:

$$K_{k+1} = P_{k+1|k} I^T (I P_{k+1|k} I^T + R)^{-1} \tag{36}$$

$$O_{k+1|k+1} = O_{k+1|k} + K_{k+1}(z_{k+1} - Y_{k+1}) \tag{37}$$

$$P_{k+1|k+1} = P_{k+1|k} - K_{k+1} I P_{k+1|k} \tag{38}$$

The Kalman gain K is utilized in the estimation of heart rate values for the current sliding window. $O_{k+1|k+1}$ represents the optimal heart rate value estimate of the current sliding window, while $P_{k+1|k+1}$ stands for the covariance matrix corresponding to $O_{k+1|k+1}$. If $N(N > 3)$ consecutive sliding windows exhibit the outlier heart rate observation, the Kalman filtering process will be temporarily halted. Subsequently, the process will resume by re-selecting an initial value based on the heartbeat signal within the current sliding window. The performance evaluation of the KFRV will be presented in the next section.

IV. EXPERIMENTAL RESULTS

A. EXPERIMENTAL SETUP

In this study, a Texas Instruments (TI) mm-wave AWR1642 FMCW radar was utilized in all experiments. The radar system was equipped with two transmit antennas and four receive antennas, and the data collected were transmitted to a personal computer via a USB interface for signal processing using MATLAB. The configuration parameters of the FMCW radar during the experiment are outlined in Table 2.

The experiments were conducted in a laboratory environment with twenty-five healthy volunteers (thirteen males and twelve females). During experiments, volunteers were positioned directly in front of the radar while undergoing body movements during monitoring. The Polar H10 chest heart rate sensor was utilized as a reference in the experiments, as illustrated in Fig.12. The data of each volunteer were collected in groups of 1200 frames, with a duration of 60 s per group, based on a frame frequency of 20 Hz. For heart rate detection, the parameters of the sliding window were set

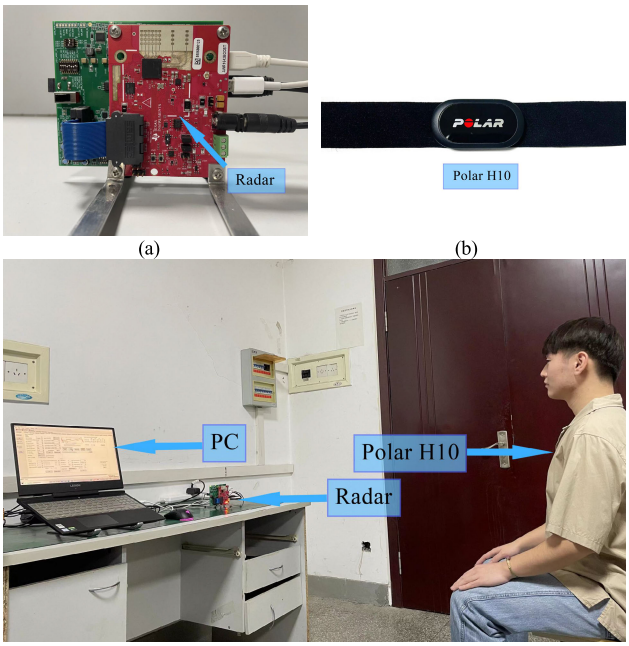

FIGURE 12. Heart rate monitoring experiments. (a) FMCW radar. (b) Polar H10 chest heart rate sensor (c) Experimental scenarios.

to a window size of 25.6 s and a step size of 1 s. To ensure simultaneous data collection from the radar and heart rate sensor, the reference heart rate data were obtained through the initiation of the Polar H10 chest heart rate sensor acquisition process at the start of vital sign data collection. The Polar H10 chest heart rate sensor provided updated heart rate values every second throughout the data collection process.

The Mean Absolute Error (MAE) is adopted for evaluating the heart rate estimation accuracy of different schemes, and MAE can be written as

$$MAE = \frac{\sum_{i=1}^{N} |BPM_{true}(i) - BPM_{est}(i)|}{N} \tag{39}$$

where MAE is the summation of the absolute differences between the reference heart rate measurement BPM_{true} obtained by a Polar H10 chest heart rate sensor and the estimated heart rate BPM_{est} obtained by a scheme in N sliding windows, where N represents the total number of sliding windows in each data group.

B. MEASUREMENT RESULTS

1) VALIDATION OF THE EFFECTIVENESS OF THE APSEM METHOD

In this section, we experimentally validated the effectiveness of the APSEM method. In these experiments, we compared the performance of the EM method with the default initial distribution parameter (referred to as the EM method [26] in the table) and the APSEM method. The default initial distribution parameter was set to be $\langle a_0 = 0.3, b_0 = 0.5 \rangle$. Both methods were employed to the same set of heartbeat signals to remove motion artifacts, the heart rate was then

TABLE 3. Mae of heartbeat rate estimation.

Group	MAE without MA filtering (bpm)	MAE of the EM method (bpm)	MAE for the APSEM method (bpm)	Motion mode
1	25.97	24.71	2.11	Model 1
2	6.03	4.51	2.31	Model 2
3	14.91	4.11	2.83	Model 3
4	3.09	2.34	2.34	Model 4
5	2.89	3.94	2.80	Model 5
Average	10.58	7.92	2.48	

estimated using the scheme that combines the Rife spectral analysis method with the VME algorithm. Table 3 displays the MAE of heartbeat rate estimation for the EM method with default initial distribution parameter and the APSEM method under five human motion modes.

Results in Table 3 reveal that, when the model of human motion is Model 1 (High-level body motion), the interference of human motion on the heartbeat signal is significant. Without performing motion artifacts removal processing, the scheme which combines the Rife spectral analysis method with the VME algorithm for heart rate detection results in an error of about 26 bpm. Even for the scheme with motion artifacts removal processing using the EM method with default initial distribution parameter, the MAE of heart rate estimation for this group of signals is still very high, only improving by 1.26 bpm compared with the scheme without performing motion artifacts removal processing. However, when using the APSEM method for motion artifacts removal processing (i.e., adopting the Adaptive Parameter Selection for the EM method), the heart rate estimation accuracy for this group of signals is improved by about 22.6 bpm.

When the human motion model is Model 2 (Medium-level body motion) or Model 3 (Low-level body motion), it becomes evident that both the EM method with default initial distribution parameter and the proposed APSEM method can improve the accuracy of heart rate estimation. From the perspective of MAE, the estimation accuracy of the APSEM method can achieve 1.5 bpm improvement compared with the EM method with the default initial distribution parameter. Furthermore, in Model 5 (Almost no body motion), it becomes apparent that the EM method with default initial distribution parameter encountered a loss of approximately 1 bpm. On the other hand, the APSEM method did not result in any degradation in performance.

In summary, the EM method with default initial distribution parameter demonstrates its suitability in dealing with heartbeat signals influenced by low to medium levels of human motion. However, it cannot effectively eliminate interference caused by high-level human motion and experiences performance deterioration under stationary conditions. In contrast, the proposed APSEM method achieves better motion artifacts removal performance under all the human motion models processed in this paper and is particularly

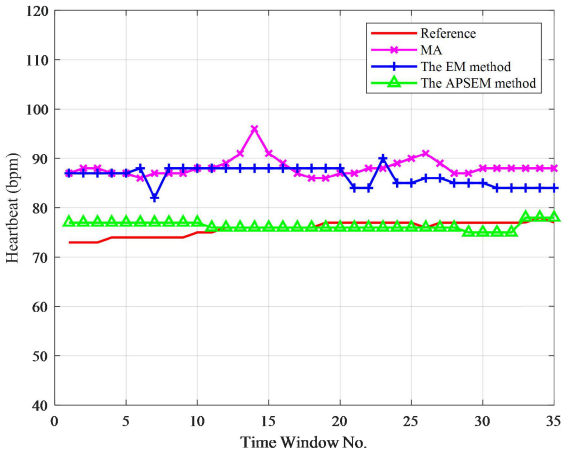

FIGURE 13. Heart rate comparison curve.

effective in dealing with interference caused by high-level human motion. It shows excellent performance in effectively eliminating interference resulting from high-level human motion. These experimental results fully demonstrate that the APSEM method outperforms the EM method in motion artifacts removal.

Fig.13 displays the comparison of the heart rate curve obtained by employing different schemes in the presence of human motion. The reference heart rate curve of a subject was recorded using a Polar H10 chest heart rate sensor and is depicted by the red curve. The heart rate curve adopting the VME algorithm and the Rife spectral analysis method without removing motion artifacts is plotted by the purple curve. The heart rate curve, obtained by applying the VME algorithm and Rife spectral analysis method to the signal filtered for MA using the EM method with default initial distribution parameter, is depicted in the blue curve. The green curve shows the performance of heart rate detection by exploiting the scheme which combines the APSEM method with the Rife spectral analysis method and the VME algorithm.

Upon analyzing the trend of heart rate changes, it is evident that the green heart rate curve closely resembles the red reference heart rate curve. Conversely, the purple heart rate curve exhibits considerable deviations from the reference heart rate curve. Further comparison of the purple and blue curves reveals that the EM method with default initial distribution parameters can suppress MA, but the effect is not significant. The MAE of the purple curve is 12.34 bpm (without performing MA filtering out processing), while the MAE of the blue curve is 10.57 bpm (employing the EM method with default initial distribution parameter), compared to the reference heart rate. The improvement in heart rate detection (MAE) achieved by the EM method with default initial distribution parameter is only about 1.8 bpm as compared to the case without performing MA filtering out processing.

However, the green curve obtained by employing the scheme which combines the APSEM method with the Rife

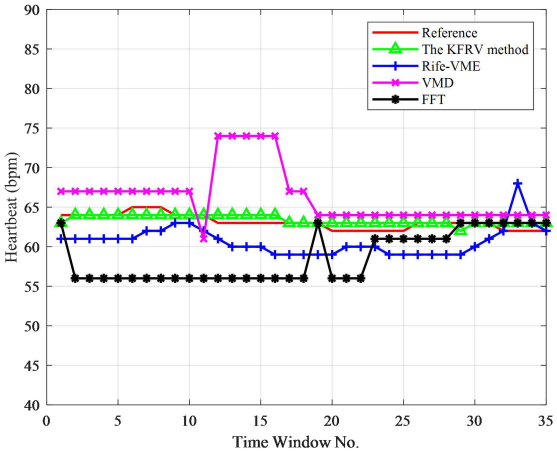

FIGURE 14. Heart rate comparison curve.

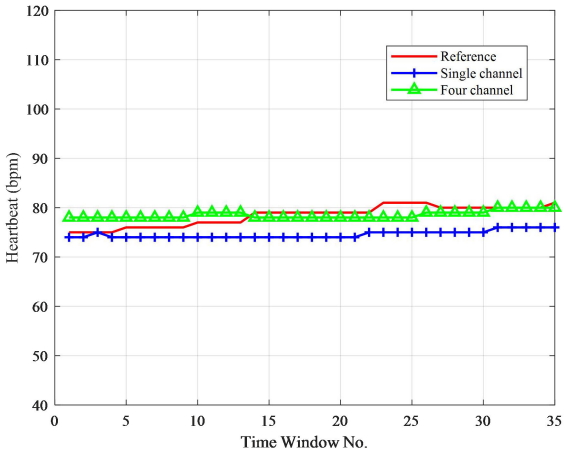

FIGURE 15. Heart rate comparison curve.

spectral analysis method and VME algorithm is noticeably closer to the reference heart rate curve, with an MAE of 1.49 bpm. This represents an improvement of 9.08 bpm over the blue curve and underscores the effectiveness of the APSEM method in heart rate detection in the presence of human motion as compared to the EM method with default initial parameters. These experimental results further demonstrate the superiority of the proposed APSEM method in suppressing interference caused by human motion.

2) VALIDATION OF THE EFFECTIVENESS OF THE KFRV METHOD

In this section, we experimentally validated the effectiveness of the KFRV method. To ensure the fairness of the performance comparison, the APSEM method was employed to filter out motion artifacts from the heartbeat signals before using different methods to estimate heart rate.

Fig.14 illustrates the comparison of heart rate estimation results obtained from different schemes. The black curve represents the heart rate estimated by the FFT spectral analysis method. The purple curve represents the heart rate estimated by the scheme that combines the FFT spectral analysis method with the VMD algorithm. The blue curve represents the heart rate estimated by the scheme that combines the Rife spectral analysis method with the VME algorithm, while the green curve represents the heart rate estimated by the KFRV method.

As observed from the figure, the black, purple, and blue curves exhibit some degree of heart rate deviation, with the MAE of 4.69 bpm, 3.43 bpm, and 2.83 bpm, respectively. This deviation is attributed to the effect of random disturbances that cannot be eliminated by the spectral analysis method. In contrast, the green curve shows that the heart rate change tendency conforms to the reference heart rate curve, with an MAE of only 0.57 bpm. This represents a significant improvement of 4.12 bpm over the black curve, 2.86 bpm over the purple curve, and 2.26 bpm over the blue curve, indicating that the KFRV method can effectively suppress random disturbances, and enhance the accuracy and stability of heart rate detection. In addition, by further comparing the black curve and the green curve, it can be concluded that even after employing the APSEM method to filter out motion artifacts, utilizing only the FFT spectral analysis method for heart rate estimation still results in significant errors. However, when the KFRV method is employed after the APSEM method, it effectively reduces the errors in heart rate estimation. This further demonstrates the effectiveness of the KFRV method in improving the accuracy of heart rate detection.

3) VALIDATION OF THE EFFECTIVENESS OF MCA

To evaluate the benefits of the MCA scheme utilizing multiple receiver antennas, experiments were conducted to compare the performance of the proposed scheme that combines the APSEM method with the KFRV method applied to both single-channel data and multi-channel data. Fig.15 displays the heart rate change curves obtained from exploiting the proposed scheme to single-channel data, as well as to four channels of data processed by MCA and then exploiting the proposed scheme.

The blue and green curves respectively represent the heart rate change curves obtained from the proposed scheme applied to single-channel data and four-channel data. As evidenced by Fig.15, the green curve closely approximates the reference heart rate curve compared to the blue curve. The MAE of the blue curve is 3.83 bpm, whereas the MAE of the green curve is 1.57 bpm, indicating that using multi-channel data for MCA processing improves the heart rate detection performance by 2.3 bpm. This experimental result confirms the superiority of the MCA scheme utilizing multiple receiver antennas.

4) COMPARISON OF PERFORMANCE BETWEEN DIFFERENT SCHEMES OF HEART RATE DETECTION IN THE PRESENCE OF HUMAN MOTION

In this section, we provide a comparative analysis of various heart rate detection schemes. Fig.16 and Table 4 present the results of the comparison, which includes the proposed

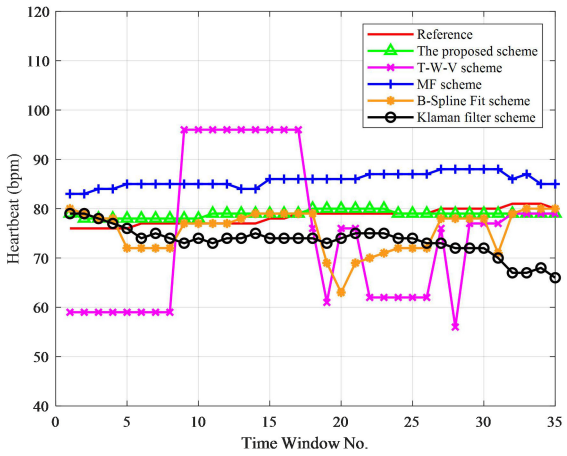

FIGURE 16. Heart rate comparison curve.

scheme that utilizes MCA, APSEM, and KFRV methods, as well as the time-window-variation (T-W-V) scheme presented in [11], the MF scheme presented in [22], the B- Spline Fit scheme presented in [24], and the Kalman filter scheme presented in [34]. The experiments for heart rate detection were conducted with 25 volunteers in the presence of human motion, who was seated and facing toward a radar.

Fig.16 illustrates the heart rate curves for one of the 25 groups for heart rate detection results. The red curve represents the reference heart rate measured by the Polar H10 chest heart rate sensor. The green curve represents the heart rate curve obtained by employing the proposed scheme, while the purple curve corresponds to the heart rate curve obtained by employing the T-W-V scheme. The blue curve represents the heart rate curve obtained by employing the MF scheme, and the orange curve represents the heart rate curve obtained by employing the B-Spline Fit scheme. Finally, the black curve represents the heart rate curve obtained by employing the Kalman filter scheme.

The analysis of Fig.16 reveals that the heart rate curve obtained by the proposed scheme closely resembles the reference heart rate curve and exhibits a similar trend in heart rate variations. Conversely, the heart rate curves obtained by employing the other schemes show remarkable deviation from the reference heart rate curve. Additionally, the MAE of the proposed scheme for this group of data is 1.26 bpm, whereas the T-W-V scheme has an MAE of 13.2 bpm, the MF scheme has an MAE of 7.43 bpm, the B-Spline Fit scheme has an MAE of 3.71 bpm, and the Kalman filter scheme has an MAE of 5.4 bpm. These results further emphasize the superior accuracy of the proposed scheme compared to the other four traditional heart rate detection schemes.

The complete representation of the MAE for the 25 groups of heart rate results obtained by the five previously mentioned heart rate detection schemes is presented in Table 4. As indicated in Table 4, the proposed scheme achieved an average MAE of 1.56 bpm for the 25 obtained heart rate results, outperforming the T-W-V scheme, the MF scheme, the B-spline scheme, and the Kalman filter scheme, which exhibited average MAEs of 10.43 bpm, 4.15 bpm, 4.68 bpm, and 5.70 bpm, respectively. Notably, the proposed scheme demonstrated significant improvements over the T-W-V, MF, B-Spline Fit, and Kalman filter schemes, reducing the MAE by approximately 8.9 bpm, 2.6 bpm, 3.1 bpm, and 4.1 bpm, respectively.

The T-W-V scheme performs poorly in heart rate detection under human motion, with a maximum MAE of 26.66 bpm and a minimum of 1.49 bpm. Furthermore, the MAEs of the T-W-V scheme are generally higher than other schemes in the comparative experiments. Although the MF scheme shows relatively good performance in some sets of data, its performance for heart rate detection in the presence of human motion is not stable, as indicated by the maximum MAE of 20.06 bpm and the minimum MAE of 1.26 bpm in the table. Similarly, the performance of the B-Spline Fit scheme and the Kalman filter scheme in heart rate detection under human motion is also unstable. The maximum MAE of the B-Spline Fit scheme is 17.94 bpm, and the minimum MAE is 1.49 bpm. The maximum MAE of the Kalman filter scheme is 24.63 bpm, and the minimum MAE is 0.49 bpm.

In contrast, the proposed scheme delivered a stable MAE of approximately 1.4 bpm, with a maximum of no more than 2.5 bpm and a minimum of 0.57 bpm. The standard deviation of the MAE for the 25 obtained heart rate results was 0.56 for the proposed scheme, 6.66 for the T-W-V scheme, 4.74 for the MF scheme, 4.05 for the B-Spline Fit scheme, and 5.89 for the Kalman filter scheme, which indicates that the proposed scheme exhibits higher heart rate detection stability compared to the other four traditional schemes.

Based on the above analysis of extensive experimental results, it can be concluded that the proposed scheme offers higher accuracy and stability for heart rate detection in the presence of human motion compared to the traditional schemes. Furthermore, the results of the experiments, as depicted in Table 4, demonstrate the high accuracy and reliability of the proposed scheme for non-contact heart rate detection in the presence of human motion.

5) COMPARISON OF PERFORMANCE BETWEEN DIFFERENT SCHEMES OF HEART RATE DETECTION IN A STATIC STATE

The experimental results above demonstrate the excellent performance of the proposed scheme for heart rate detection in the presence of human motion. To validate the applicability of the proposed scheme for heart rate detection in a static state, we compared the heart rate detection performance of the proposed scheme with the latest VMD-based heart rate detection scheme.

Table 5 shows the comparison results of the proposed scheme and the latest VMD-based scheme for heart rate detection in a static state. As demonstrated by Table 5, the proposed scheme resulted in an average MAE of 0.99 bpm in detecting heart rate, while the utilization of the VMD-based scheme resulted in an average MAE of 0.74 bpm. It is worth noting that there is only a difference of about 0.25 bpm in

TABLE 4. Estimation results adopting different schemes in the presence of human motion.

Subject	Gender	MAE for the proposed scheme (bpm)	MAE for the T-W-V scheme in [11] (bpm)	MAE for the MF scheme in [22] (bpm)	MAE for the B-Spline Fit scheme in [24] (bpm)	MAE for the Kalman filter scheme in [34] (bpm)
1	Female	0.91	6.69	1.34	4.34	2.71
2	Female	1.40	8.89	3.94	2.46	2.74
3	Female	1.91	15.23	3.43	6.71	6.46
4	Female	1.23	3.40	1.74	2.20	0.80
5	Female	1.23	5.17	1.26	1.66	1.26
6	Female	1.09	2.69	3.54	6.11	3.91
7	Female	2.34	10.51	3.91	6.03	8.14
8	Female	2.00	16.49	2.17	2.94	4.54
9	Female	1.06	6.89	9.43	15.00	9.80
10	Female	2.40	13.20	1.49	2.54	12.23
11	Female	2.43	9.51	2.17	3.69	5.00
12	Female	1.03	3.06	1.31	1.60	3.17
13	Male	0.57	5.60	2.34	2.77	1.37
14	Male	1.37	8.29	2.20	2.97	1.97
15	Male	1.34	2.00	1.26	2.03	1.54
16	Male	0.74	7.37	1.94	1.91	1.31
17	Male	1.26	13.20	7.43	3.71	5.40
18	Male	1.94	7.43	2.57	4.54	4.94
19	Male	1.20	1.49	1.51	2.26	0.49
20	Male	2.17	14.49	1.80	3.94	2.00
21	Male	1.86	17.86	3.49	1.49	2.14
22	Male	2.31	21.60	2.46	5.69	24.63
23	Male	1.29	12.23	20.06	9.09	12.49
24	Male	1.60	20.86	16.89	17.94	18.37
25	Male	2.26	26.66	4.03	3.34	4.97
Average		1.56	10.43	4.15	4.68	5.70
Standard deviation		0.56	6.66	4.74	4.03	5.87

TABLE 5. Estimation results adopting two different schemes in a static state.

Subject	MAE for the proposed scheme (bpm)	MAE for the VMD-based scheme (bpm)
1	0.77	0.57
2	1.37	1.43
3	1.06	0.69
4	0.76	0.34
5	0.97	0.68
Average	0.99	0.74

the MAE between the two schemes for heart rate detection in a static state. Although the heart rate estimation accuracy of the proposed scheme is a little bit worse than the VMD-based scheme under a static state, it still achieves high detection accuracy overall. These experimental results indicate that the proposed scheme is also applicable for heart rate detection in a static state.

6) VALIDATION OF THE EFFECTIVENESS OF THE PROPOSED SCHEME IN DETECTING RAPID HEART RATE VARIATIONS

After validating the superior detection performance of the proposed scheme in both human motion and static states, we conducted a validation study using data that involved rapid variations in the subject's heart rates. Fig.17 illustrates the heart curve obtained employing the proposed scheme when the subject experienced rapid changes in heart rate. The red

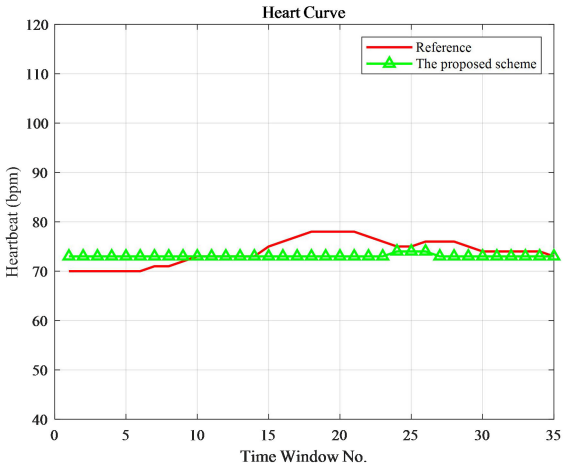

FIGURE 17. Heart rate curve.

curve represents the reference heart rate curve, while the green curve represents the heart rate curve obtained employing the proposed scheme. From the figure, it is evident that the green curve does not accurately track the true trend of the subject's heart rate changes compared to the reference curve when rapid heart rate variations occur. This suggests that the proposed scheme does not achieve optimal tracking of rapidly changing heart rates. However, when considering the measurement error of heart rate detection, MAE for the heart rate results obtained employing the proposed scheme

for this dataset is 2.17 bpm. This experimental result demonstrates that the proposed scheme still maintains a high level of accuracy in heart rate detection.

V. DISCUSSION

This paper presents a non-contact heart rate detection scheme based on millimeter-wave radar. Experimental results have demonstrated that the proposed scheme can provide highly accurate heart rate estimation in scenarios where the human subject is either stationary or in the presence of body movements. However, there are certain limitations to the proposed scheme that need to be discussed in this section.

Firstly, the body movements considered in this study are limited to upper body swings, head shakes, and hand raises when the human subject maintains an upright position facing the radar. In practical applications, the detection scenarios for vital signs can be more complex, such as when the human body is in a lying, side, or back position. Therefore, further consideration is required to determine whether the proposed scheme applies to more complex environments and potential challenges. Secondly, in practical vital sign monitoring, the heart rate of the subject may experience drastic changes within a short time due to certain emergencies. However, the heart rate tracking method employed in the proposed scheme, which relies on Kalman filtering, may not accurately track the true trend of the subject's heart rate during rapid changes. Hence, future research should focus on how to detect rapidly changing heart rates.

Considering the above limitations of the proposed scheme, the suggested application scenario is a relatively stable environment where the subject faces the radar while being stationary or in the presence of body movements.

VI. CONCLUSION

In this paper, a new scheme for heart rate detection is proposed, which is based on 77 GHz FMCW radar. In order to cope with human motion artifacts, we propose the Adaptive Parameter Selection for Expectation-Maximization (APSEM) method. This method improves the accuracy and robustness of motion artifacts filtering by adding an adaptive initial distribution parameter selection to the traditional EM method. Additionally, we propose a novel heart rate detection sub-framework after the APSEM method for further dealing with interference which is called the KFRV method. This sub-framework combines Kalman filtering with the Rife spectral analysis method and the VME algorithm to effectively suppress random disturbances such as impulse noise and random body movements. As a result, heart rate estimation accuracy can be further improved.

Based on these above methods, we propose a novel heart rate detection scheme by adopting MCA, APSEM, and KFRV methods. We validate the effectiveness of the proposed scheme through extensive experiments. The proposed scheme is evaluated by using heartbeat signals obtained from 25 volunteers in the presence of human motion, and the results show that the MAE of heart rate detection is less than 2.5 bpm. Compared to traditional schemes, the proposed scheme offers higher accuracy and stability for heart rate detection in the presence of human motion. The proposed scheme is further tested on multiple volunteers in a static state, demonstrating an average MAE of 0.99 bpm in detecting heart rate. In conclusion, the proposed MCA-APSEM-KFRV scheme enhances the accuracy and robustness of heart rate detection by effectively filtering out motion artifacts and suppressing random disturbances. And the extensive experimental results demonstrate the applicability of the proposed scheme for accurate heart rate detection in both human motion and static states.

REFERENCES

[1] E. Khan, F. Al Hossain, S. Z. Uddin, S. K. Alam, and M. K. Hasan, "A robust heart rate monitoring scheme using photoplethysmographic signals corrupted by intense motion artifacts," *IEEE Trans. Biomed. Eng.*, vol. 63, no. 3, pp. 550–562, Mar. 2016.

[2] M. Kebe, R. Gadhafi, B. Mohammad, M. Sanduleanu, H. Saleh, and M. Al-Qutayri, "Human vital signs detection methods and potential using radars: A review," *Sensors*, vol. 20, no. 5, p. 1454, Mar. 2020.

[3] W. Zhang, G. Li, Z. Wang, and H. Wu, "Non-contact monitoring of human heartbeat signals using mm-wave frequency-modulated continuous-wave radar under low signal-to-noise ratio conditions," *IET Radar, Sonar Navigat.*, vol. 16, no. 3, pp. 456–469, Mar. 2022.

[4] P. Zhao, C. X. Lu, B. Wang, C. Chen, L. Xie, M. Wang, N. Trigoni, and A. Markham, "Heart rate sensing with a robot mounted mmWave radar," in *Proc. IEEE Int. Conf. Robot. Autom. (ICRA)*, May 2020, pp. 2812–2818.

[5] W. Lv, Y. Zhao, W. Zhang, W. Liu, A. Hu, and J. Miao, "Remote measurement of short-term heart rate with narrow beam millimeter wave radar," *IEEE Access*, vol. 9, pp. 165049–165058, 2021.

[6] X. Yang, B. Yang, Z. Wang, Y. Zhang, H. Zhou, X. Li, and S. Cao, "Progress in clinical application of non-contact vital signs monitoring technology," *Med. Inf.*, vol. 31, no. 18, pp. 41–44, Sep. 2018.

[7] Y. Jing, Y. Cao, M. Zhu, T. Lei, J. Xia, Z. Li, L. Zhang, J. Wang, and G. Lu, "Research status and development of non-Contact life detection technology," *China Med. Devices*, vol. 36, no. 6, pp. 1–4, 2021.

[8] P. Hou, N. Li, and T. Song, "Research status and development of life detection technology," *Transducer Microsyst. Technol.*, vol. 33, no. 7, pp. 1–8, 2014.

[9] J. Li, L. Liu, Z. Zeng, and F. Liu, "Advanced signal processing for vital sign extraction with applications in UWB radar detection of trapped victims in complex environments," *IEEE J. Sel. Topics Appl. Earth Observ. Remote Sens.*, vol. 7, no. 3, pp. 783–791, Mar. 2014.

[10] Z. Yang, P. H. Pathak, Y. Zeng, X. Liran, and P. Mohapatra, "Vital sign and sleep monitoring using millimeter wave," *ACM Trans. Sensor Netw.*, vol. 13, no. 2, pp. 1–32, May 2017.

[11] J. Tu and J. Lin, "Fast acquisition of heart rate in noncontact vital sign radar measurement using time-window-variation technique," *IEEE Trans. Instrum. Meas.*, vol. 65, no. 1, pp. 112–122, Jan. 2016.

[12] J.-M. Muñoz-Ferreras, J. Wang, Z. Peng, R. Gómez-García, and C. Li, "From Doppler to FMCW radars for non-contact vital-sign monitoring," in *Proc. 2nd URSI Atlantic Radio Sci. Meeting (AT-RASC)*, Jun. 2018, pp. 1–4.

[13] J. M. Munoz-Ferreras, Z. Peng, R. Gomez-Garcia, and C. Li, "Random body movement mitigation for FMCW-radar-based vital-sign monitoring," in *Proc. IEEE Topical Conf. Biomed. Wireless Technol., Netw., Sens. Syst.*, 2016, pp. 22–24.

[14] R. Ernst, E. Nilsson, and P. A. Viberg, "60 GHz vital sign radar using 3D-printed lens," in *Proc. IEEE Sensors*, Oct. 2017, pp. 1–3.

[15] H. Lee, B.-H. Kim, J.-K. Park, S. W. Kim, and J.-G. Yook, "A resolution enhancement technique for remote monitoring of the vital signs of multiple subjects using a 24 Ghz bandwidth-limited FMCW radar," *IEEE Access*, vol. 8, pp. 1240–1248, 2020.

[16] F. Zhen, J. Pu, Z. Hao, Y. A. O. Yicheng, G. E. N. G. Fanglin, L. I. U. Changyu, Y. A. N. Baiju, W. A. N. G. Peng, D. U. Lidong, and C. H. E. N. Xianxiang, "Review of noncontact medical and health monitoring technologies based on FMCW radar," *J. Radars*, vol. 11, no. 3, pp. 499–516, 2022.

[17] M. E. Torres, M. A. Colominas, G. Schlotthauer, and P. Flandrin, "A complete ensemble empirical mode decomposition with adaptive noise," in *Proc. IEEE Int. Conf. Acoust., Speech Signal Process. (ICASSP)*, May 2011, pp. 4144–4147.
[18] K. Wang, Y. Zhao, and J. Fang, "Separation and denoising of respiratory heartbeat signals based on millimeter-wave radar," in *Proc. IEEE 4th Int. Conf. Power, Intell. Comput. Syst. (ICPICS)*, Jul. 2022, pp. 950–954.
[19] K. Dragomiretskiy and D. Zosso, "Variational mode decomposition," *IEEE Trans. Signal Process.*, vol. 62, no. 3, pp. 531–544, Feb. 2014.
[20] P. Zheng, C. Zheng, X. Li, H. Chen, A. Wang, and Y. Luo, "Second harmonic weighted reconstruction for non-contact monitoring heart rate," *IEEE Sensors J.*, vol. 22, no. 6, pp. 5815–5823, Mar. 2022.
[21] P. Zhou, Y. Xu, X. Wang, H. Xu, X. Shi, and X. Li, "Design of vital signs detection system based on 77GHz FMCW radar," in *Proc. Int. Conf. Microw. Millim. Wave Technol. (ICMMT)*, Aug. 2022, pp. 1–3.
[22] Q. Lv, L. Chen, K. An, J. Wang, H. Li, D. Ye, J. Huangfu, C. Li, and L. Ran, "Doppler vital signs detection in the presence of large-scale random body movements," *IEEE Trans. Microw. Theory Techn.*, vol. 66, no. 9, pp. 4261–4270, Sep. 2018.
[23] Q. Wu, Z. Mei, Z. Lai, D. Li, and D. Zhao, "A non-contact vital signs detection in a multi-channel 77 GHz LFMCW radar system," *IEEE Access*, vol. 9, pp. 49614–49628, 2021.
[24] F. Wang, X. Zeng, C. Wu, B. Wang, and K. J. R. Liu, "Driver vital signs monitoring using millimeter wave radio," *IEEE Internet Things J.*, vol. 9, no. 13, pp. 11283–11298, Jul. 2022.
[25] M. Alizadeh, G. Shaker, J. C. M. D. Almeida, P. P. Morita, and S. Safavi-Naeini, "Remote monitoring of human vital signs using mm-wave FMCW radar," *IEEE Access*, vol. 7, pp. 54958–54968, 2019.
[26] S. U. Pillai, *Array Signal Processing*. New York, NY, USA: Springer, 2012.
[27] J.-A. Ting, E. Theodorou, and S. Schaal, "A Kalman filter for robust outlier detection," in *Proc. IEEE/RSJ Int. Conf. Intell. Robots Syst.*, Nov. 2007, pp. 1514–1519.
[28] Z. Mei, "Non-contact vital signs detection technology based on millimeter wave radar," M.S thesis, Dept. Inf. Sci. Eng., Southeast Univ., Jiangsu, China, 2022.
[29] J. K. Kruschke, "Bayesian data analysis," *Wiley Interdiscip. Rev. Cogn. Sci.*, vol. 1, no. 5, pp. 658–676, 2010.
[30] S. Ji, "Research on vital signs detection technology based on millimeter wave radar," M.S thesis, Dept. Mech. Eng., Southeast Univ., Jiangsu, China, 2022.
[31] M. Nazari and S. M. Sakhaei, "Variational mode extraction: A new efficient method to derive respiratory signals from ECG," *IEEE J. Biomed. Health Informat.*, vol. 22, no. 4, pp. 1059–1067, Jul. 2018.
[32] D. C. Rife and G. A. Vincent, "Use of the discrete Fourier transform in the measurement of frequencies and levels of tones," *Bell Syst. Tech. J.*, vol. 49, no. 2, pp. 197–228, Feb. 1970.
[33] Z. Chen, Y. Liu, and Z. Cai, "Noncontact heart rate detection method based on Kalman filter," in *Proc. Global Rel. Prognostics Health Manag. (PHM-Yantai)*, Oct. 2022, pp. 1–5.
[34] M. Arsalan, A. Santra, and C. Will, "Improved contactless heartbeat estimation in FMCW radar via Kalman filter tracking," *IEEE Sensors Lett.*, vol. 4, no. 5, pp. 1–4, May 2020.
[35] Y. He, *Radar Data Processing With Applications*. Beijing, China: House of Electronics Industry, 2016.

ZEKUN CHEN (Member, IEEE) received the B.S. degree from Yantai University, Yantai, China, in 2020, where he is currently pursuing the master's degree with the School of Physics and Electronic Information. His current research interests include radar signal processing and vital sign detection.

YUNXUE LIU received the Ph.D. degree from Shandong University, Jinan, China, in 2009. He is currently a Full Professor with the School of Physics and Electronic Information, Yantai University, Yantai, China. His current research interests include millimeter wave radar signal processing, high-speed signal real-time processing, electronic counter-measures, and cognitive radio.

CHENHONG SUI (Member, IEEE) received the Ph.D. degree from the School of Electronic Information and Communications, Huazhong University of Science and Technology, Wuhan, China, in 2015. She is currently an Associate Professor with the School of Physics and Electronic Information, Yantai University, Yantai, China. Her current research interests include remote sensing image processing, computer vision, and image quality assessment.

MIN ZHOU received the B.S. degree from Yantai University, Yantai, China, in 2021, where she is currently pursuing the master's degree with the School of Physics and Electronic Information. Her current research interests include radar signal processing and vital sign detection.

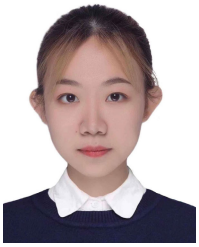

YUQING SONG received the B.S. degree from Yantai University, Yantai, China, in 2021, where she is currently pursuing the master's degree with the School of Physics and Electronic Information. Her current research interests include signal denoising and vital sign detection.